Chemical Engineering Journal 155 (2009) 388–395

Contents lists available at ScienceDirect

Chemical Engineering Journal

journal homepage: www.elsevier.com/locate/cej

Particle loading in a catalyst-trap microreactor: Experiment vs. simulation

J. Huang, J. Weinstein, R.S. Besser*

Department of Chemical Engineering and Materials Science, Stevens Institute of Technology, Castle Point on Hudson, Hoboken, NJ 07030, USA

ARTICLE INFO

Article history:
Received 27 May 2009
Received in revised form 24 July 2009
Accepted 27 July 2009

Keywords:
Microreactor
Catalyst loading
Pd/C
Grain size distribution
Catalyst trap

ABSTRACT

We present the results of a study of the catalyst loading behavior on the "catalyst-trap" microreactor, a novel microreactor recently reported by McGovern et al. (2008) [1]. The study focuses on the important issue of catalyst deployment inside microscale reactors which must be understood in order to further the implementation of emerging microtechnology for organic chemical synthesis. We initially set out to use the catalyst-trap microreactor to investigate the catalytic hydrogenation of 3-nitrotoluene. In that investigation a 100% yield was fortuitously achieved due to the activity of the reaction. However, the low trap occupancy ratio (20% of the traps had been loaded) could still be an impediment, especially for other more complex reactions. After extensively studying the loading procedure, 98% of the traps in the reactor were able to be successfully loaded. Simulations based on a random-walk model and the procedures of the loading experiments were conducted to better understand the filling mechanism. We found the physical catalyst loading procedure was consistent with the simple mechanism in our simulations. Through this work, catalytic area and catalytic efficiency have been significantly increased, and the synthetic capability enhanced as a result.

1. Introduction

Multiphase miniaturized chemical reaction, which first started to appear [2] in the late 1990s, offers a new technique for organic synthesis, and is widely applicable to the hydrogenation and dehydrogenation of hydrocarbons [3], arylation [4] reaction and enzymatic synthesis [5], and even recently has found applicable in lithium–halogen exchange reaction [6]. Genomic sequencing study [7] is one of the most current applications of this technique. Miniaturization aims to economize the use of materials, facility resources and synthetic manipulations while producing safer chemical transformations at higher yields with fewer or no unwanted by-products [8]. Advantages of microscale systems include superior mass and heat transport [9,10] due to large surface-to-volume ratios, continuous operation, faster reaction of unstable intermediates, as well as improved selectivity [11], reaction rate, yield and safety [3,12].

Today's growing emphasis on efficient use of chemical reagents, laboratory space for equipment and automation [13,14] in the chemical industry motivates the development of microscale chemical technologies. A major goal of chemical process miniaturization is the design and fabrication of microscale reactor chips capable of more efficiently introducing reagents into a reaction chamber, mixing [15], reacting, purifying new intermediates and products for in vitro and in vivo [16] assay in preliminary pharmaceutical drug-discovery [17]. As today's integrated circuits evolved from vacuum-tube electronics [18], microscale reactor chips are analogously are evolving from conventional reactors.

Our work was focused on a microfabricated silicon chip mounted on a heating block, seen in Fig. 1(a), containing thousands of catalyst traps formed by Deep Reactive Ion Etching (DRIE) [1]. The catalyst-trap design is specifically developed for three-phase hydrogenation reactions, since nearly 20% of all reaction steps in a typical fine chemical synthesis are catalytic multiphase hydrogenations [1,19]. Different from a packed bed microreactor where packed catalysts generate high-pressure drops across the channels [19], this design allows a minimum pressure drop across the reactor system, since the traps are allow the catalyst particles to remain in fixed positions at a prescribed spacing from one another.

1.1. Catalyst-trap microreactor design

In the catalyst-trap microreactor, hydrogen is fed into the two gas channels adjacent to the liquid inlet where the reagent dissolved in the solvent is pumped (see Fig. 1(b)). The slotted walls allow a one-way movement of hydrogen (~50 psig) to dissolve from the gas channels into the reaction chamber, without liquid (~30 psig) backflow into the gas channels due to the pressure difference. The reaction chamber contains a 3399-trap array, with each trap formed as a trapezoidal arrangement of four posts that taper slightly from their uppermost surface down to the wafer surface. This design is created with the intention of holding approximately 30 catalyst particles per trap. The required particles are to be captured

* Corresponding author. Tel.: +1 201 216 5256; fax: +1 201 216 8306.
E-mail address: Ronald.Besser@stevens.edu (R.S. Besser).

1385-8947/$ – see front matter © 2009 Elsevier B.V. All rights reserved.
doi:10.1016/j.cej.2009.07.046

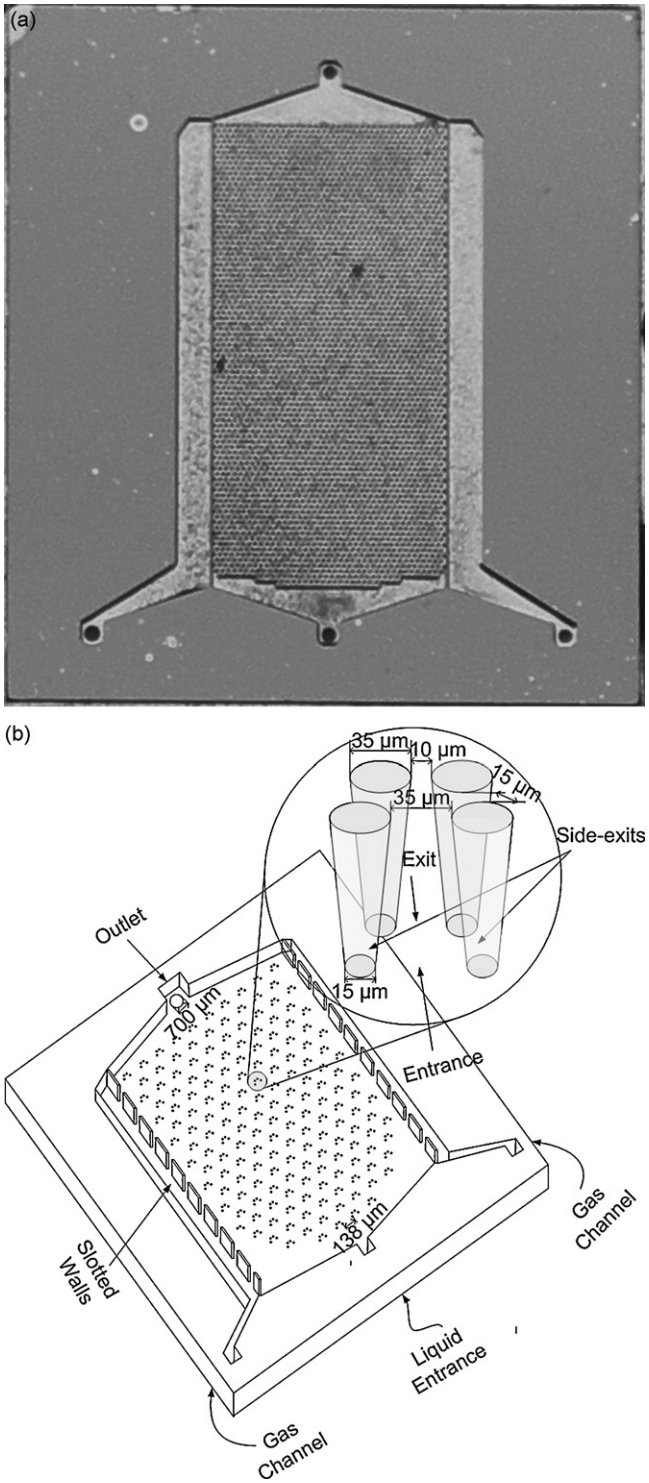

Fig. 1. (a) Micrograph of catalyst-trap microreactor chip. The reactor is 27 mm × 30 mm; the catalytic reaction area is 10 mm × 18 mm. (b) The catalyst-trap microreactor inner structure. There are one liquid entrance and two gas entrances for multiphase reactions. The gas channel is separated from the catalytic reaction zone by a slotted wall. There are 3399 traps which are designed to capture the catalyst particles individually.

by the traps during the catalyst loading procedure and to stay in place during the entire reaction process due to the direction of fluid flows.

A resistive heating block under the silicon microreactor maintains the reaction temperature. Due to the excellent thermal characteristics of microscale reactors, heat build up is discouraged favoring fewer side-products compared to traditional batch approaches.

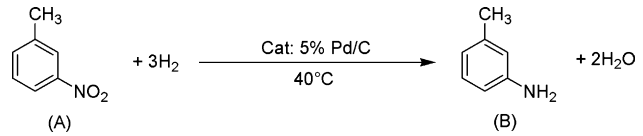

Fig. 2. The reaction scheme for 3-nitrotoluene hydrogenation. The reaction was conducted at 40 °C with 5% Pd/C catalyst within the microreactor.

1.2. Application of catalyst-trap microreactor and study motivation

As indicated in Fig. 2, the catalyst-trap reactor was used for the hydrogenation of 3-nitrotoluene (A) to 3-aminotoluene (B). The particles of 5% palladium on carbon (5 wt.% Pd/C) were loaded into the traps. Hydrogen was introduced into the gas channels, while (A) dissolved in methanol (10 wt.%) was pumped into the liquid inlet.

After allowing a suitable time for the flow system to stabilize and for the reaction to achieve steady state at 40 °C, essentially 100% (B) was obtained from a back pressure regulator connected to the outlet of the microreactor. Samples were analyzed by High-Performance Liquid Chromatography (HPLC) (see Fig. 3): [Phoenix Co. Reverse phase C-18, 4u; Mobile phase, gradient elution: 0.01NH_4OAc in H_2O/MeOH (8/2, v/v) and NH_4OH in H_2O/MeCN/MeOH (5/3/2, v/v/v)]; Mass Spectrometry (MS) and Nuclear Magnetic Resonance (NMR): [^{1}H NMR($CDCl_3$) δ 7.03 (dd, 1H, $J_{1,4} = J_{3,4} = 10.1$ Hz), 6.57 (d, 1H, $J = 7.6$ Hz H3), 6.52–6.48 (m, 3H, Ar), 3.57 (bs, 2H, NH_2), 2.26 (s, 3H, ArMe)].

Although the catalyst-trap microreactor reduced (A)–(B) in 100% yield, catalyst loading into the traps was not without difficulty. The trap use ratio, defined as the percentage of the reactor's traps utilized, was only ≈20%, although this did not impede the success of the reaction. The concern is that low use ratio causing less catalyst loaded could hinder the performance of other more complex or less active reactions. Hence, the purpose of this paper is to explore an effective catalyst loading process for the catalyst-trap microreactor as well as to understand the particle flow and capture distribution in the microreactor.

2. Experimental and calculation methods

2.1. Particle isolation and particle size histogram

Desired particles in the size range of 15–35 μm were initially selected for loading the reactor due to the flow direction, since the entrance of the trap for particles is 35 μm, while the side-exits and exit were 15 and 10 μm respectively, as shown in Fig. 1(b). The particles were obtained from a mixture of different sizes via sieving. Several sieves [Newark Wire Cloth, 20 μm; Hogentogler, 25 μm; Dual Manufacturing Co., 38 μm; Gilson, 45 μm] from 20 to 45 μm were investigated and 20 and 25 μm sieves were selected. As-received Pd/C catalyst was pulverized with a mortar and pestle, and added to a 25 μm sieve, then covered and connected to a 20 μm

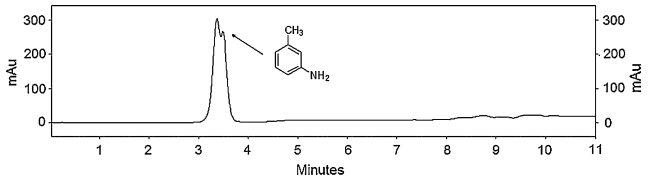

Fig. 3. The analytical HPLC results of the 3-nitrotoluene hydrogenation.

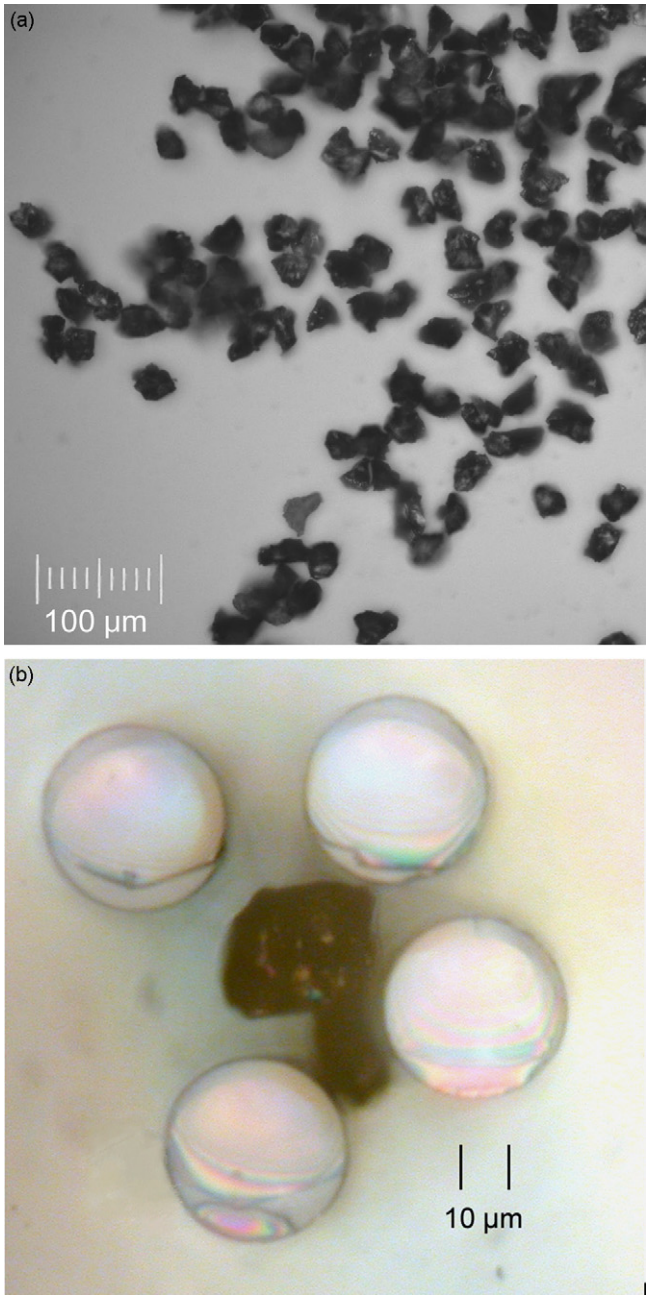

Fig. 4. Micrographs of catalyst particles (a) after sieving and (b) loaded in the traps. The catalyst particles are seen to have differing length and width in (a). Particles are appropriately sized to fit traps as seen in (b).

sieve with a receiving container below. This assembly was sealed with Parafilm® to minimize the particle loss.

The sieving process was undergoing for three times and the particles were viewed under an optical microscope [Nikon 1000, 200×] and found to be of irregular shapes (see Fig. 4(a)). To determine the dimensions of the particles, samples of the particles were photographed under the microscope. Randomly, 193 particles were chosen and measured. The maximum length and width of these particles were determined and their averages were calculated to fully describe the dimensions of the particle sample.

The particle size followed a normal distribution expressed in the histograms as shown in Fig. 5. Comparing to the entrance (35 μm) of the trap, the histograms reveal that 65% of the particles have smaller lengths than the entrance, while 95% of the particles have

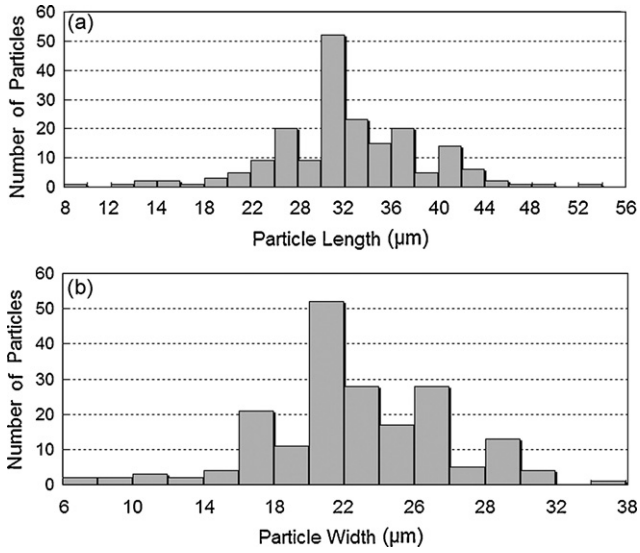

Fig. 5. Particle size histograms of (a) length and (b) width. Depending on the trap dimensions (35-μm entrance and back and side apertures of 10 and 15 μm), the histogram indicates 65% to 95% of distribution will be captured in traps.

smaller widths. Hence, the percentage of the particles which could be captured in the traps is between 65% and 95%.

Furthermore, 3.6% of the particles had a maximum length smaller than 20 μm (see Fig. 5(a)); while 31% had a maximum width larger than 25 μm (see Fig. 5(b)). This indicates the mesh size of the sieves used were not uniform. For this reason, from this point on we employed 20 and 25 μm sieve for isolation instead of 15 and 35 μm ones. Nevertheless, the particles after isolation were of the appropriate size for loading experiments and well matched the catalyst-trap dimensions (see Fig. 4(b)).

2.2. Average single particle volume calculation and density measurement

As the data in the histograms shows in Fig. 5, the mean length ($\bar{L} = 31.9\,\mu m$) and the mean width ($\bar{W} = 22.3\,\mu m$) of sized particles were obtained. The particles were defined as scalene ellipsoids [20], thus the equation of the volume calculated in the *xyz*-Cartesian coordinate system is given by

$$V_p = \frac{4}{3}\pi \cdot abc \quad (1)$$

in which a and b are the equatorial radii (along the x and y axes) and c is the polar radius (along the z-axis), respectively.

The limitation of two-dimensional micrographs allows us only two of the three parameters above. We thus arbitrarily hypothesize the measured $\bar{L}$ and $\bar{W}$ were the equatorial diameters of the ellipsoids, leaving the unknown dimension as the polar diameter, which we calculated as the average of the $\bar{L}$ and $\bar{W}$ (thus $\bar{c} = 27.1\,\mu m$). The average single particle volume V_p was found to be 10,093 μm^3.

The density (ρ) of the sieved Pd/C catalyst was determined following a simple volume replacement experiment. And it was calculated to be 0.346 g/ml. This density reflects the net density of the catalyst, including void space in the particles. This was evidenced by the fact that particles tended to float in water and other solvents that did not wet the porous network within the particles. The net particle density, which includes internal porosity, allows the determination of gross catalyst volume from knowledge of the mass without need to measure particle porosity. This density was used in calculations described below.

A catalyst particle density less than 1.0 further suggests that in many fluids, including the organic substrates typically processed

Table 1
The data collected from the seven filling experiments. The more time that was spent to fill the reactor, the more particles became trapped. However, with increased filling time, more random un-trapped free particles accumulated in the reactor. The trapping ratio obtained is useful for the calculation of the microreactor's filling efficiency.

Filling cycle	W_{in} (μg)	W_{reac} (μg)	n_{trap}	n_{free}	r_{trap}	η_{trap}
1	90	35	28	23	0.55	21.4%
2	200	130	53	21	0.72	46.6%
3	250	170	102	46	0.69	46.9%
4	315	210	113	90	0.56	37.1%
5	432	300	143	52	0.73	50.6%
6	655	490	187	79	0.70	52.6%
7	960	765	216	274	0.44	35.1%

in the catalyst-trap microreactor, there will be a tendency for a buoyancy force to exist on the particles. In gas–solid–liquid multiphase reaction scenarios, for which this reactor is intended, this force will vary based on the fractional immersion of a particle in the liquid phase. This force could play a role in perturbing particles in traps, perhaps leading to ejection from a trap. However, buoyancy forces are expected to play a diminishing role as reactor geometry and particle size decrease, since body forces such as buoyancy are less important than surface and interface interactions due to the increased surface to volume ratios of the microscale regime [21].

2.3. Experimental procedures—seven loading experiments

Seven catalyst loading experiments were performed to evaluate loading efficiency after implementing the sizing process based on our knowledge of the particle distribution. A sample size of catalyst weighing 0.75 g was prepared for loading experiments. The loading process included the following steps: (1) 50–90 mg of catalyst was placed on top of the reactor's liquid inlet hole. (2) A vacuum pump connected to a polytetrafluoroethylene (PTFE) tube, slightly larger than the diameter of the outlet, was placed over the outlet for one second to draw the particles into the reactor. The short suction time prevented un-trapped particles from prematurely leaving the reactor. (3) The reactor was manually tapped on both sides to settle the particles into traps. (4) The PTFE vacuum line was attached to the outlet to remove the un-trapped particles. (5) With a microscope, the traps were visually sampled for their contents. (6) Steps (1)–(5) were repeated seven times for each loading experiment.

During the sampling procedure 50 traps of the 3399 were examined with the microscope. These traps were uniformly distributed throughout the microreactor to assess loading over the entire device, with the same group of traps being imaged after each cycle. The microscope lens was focused to different depths in order to visualize the particle loading with elevation. The data collected from seven filling experiments are shown in Table 1. The microscope used in the loading experiments was a Nikon Eclipse ME600, at 500× magnification.

Observing Table 1, we found there are always a certain proportion of free, un-trapped particles in the reactor during the loading experiments. This proportion is defined as the trapping ratio of the reactor r_{trap}, thus:

$$r_{trap} = \frac{n_{trap}}{n_{trap} + n_{free}} \tag{2}$$

The trapping ratio is related to the trap dimensions and particle size distribution in the reactor. As seen in Table 1, this ratio varies between approximately 0.4 and 0.7. This ratio is a main factor in the filling efficiency, which describes the mass proportion between the trapped particles and total particles injected:

$$\eta_{trap} = \frac{W_{reac} \times r_{trap}}{W_{in}} \times 100\% \tag{3}$$

The variation of filling efficiency indicates the probability of immobilizing particles in the locations designed for them after multiple passes is between about 20% and 50%. This is to the exclusion of un-trapped particles remaining in the reactor that are free to escape during chemical reaction processing contributing little to conversion in steady state.

2.4. Filling experiment calculations

Total catalyst loading was assessed by determining differences in reactor mass before and after loading. The number of particles introduced into the microreactor and the number of particles trapped were calculated based on the below formulae and are plotted in Fig. 8. The total number of particles injected into the reactor was determined by knowledge of the mass injected, the catalyst density, and the average volume of a particle:

$$N_{in} = \frac{W_{in}}{\rho \times V_p} \tag{4}$$

Similarly, the total number of particles trapped was determined by the same factors combined with knowledge of the trapping ratio gained through results of imaging (Table 1):

$$N_{trap} = \frac{W_{reac} \times r_{trap}}{\rho \times V_p} \tag{5}$$

While the trapped particle count represents lower than desired efficiency of trapping (20–50% as noted from Table 1), the reactor undergoes a continuous increase in total loading with each cycle. Trapping appears to cease at the seventh cycle, when we observe a slight decline (2%) in the number of trapped particles. This also corresponds to an immediately greater proportion of free particles in the reactor in going from cycle 6 to cycle 7 (r_{trap}, Table 1), and a decrease in the overall trapping efficiency η_{trap} at the same step. We believe the explanation of these effects is that complete loading of the reactor traps has been achieved at that point.

Based on the assumption of complete filling of all 3399 traps, the capacity of an individual trap can be calculated as:

$$\text{Capacity of a single trap} = \frac{\text{total particles trapped}}{\text{number of traps}} = \frac{98,645}{3399} = 29.$$

This feature was used as a critical parameter in the simulation of catalyst loading to be described next.

3. Simulation modeling and calculation

3.1. Analogy with the Galton board

Numerical simulation was used to understand the mechanism by which individual catalyst particles enter the reactor and at some probability either become lodged in a trap, or remain outside a trap. The simulation follows the principle of the Galton board [22] since the catalyst-trap microreactor is similar in both basic structure and particle movement. The Galton board (see Fig. 6(a)) consists of a vertical chamber with interleaved rows of pins [23]. Catalyst particles were considered as analogous to the balls in the Galton board, while four-post traps were considered equivalent to the pins. A key difference between the two is that in the Galton board balls are trapped only at the bottom of the board whereas in the reactor particles can be trapped on any collision (see Fig. 6(b)). In the reactor the probabilities of the three possible movements of the particles at a given trap (to the left, to the right, or entering the trap) were calculated based on the geometry.

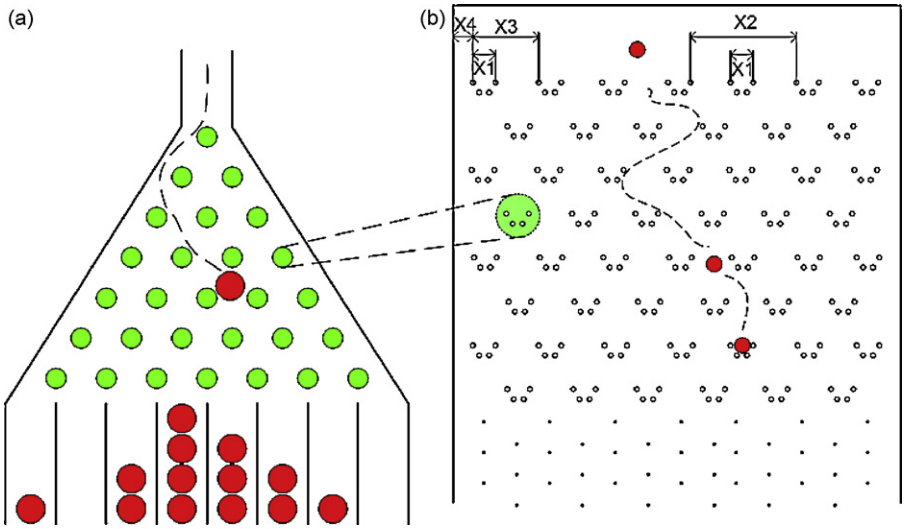

Fig. 6. The analogy of the (a) Galton board [22] and (b) microreactor inner design for simulation of the catalyst loading process as explained in the text. The microreactor model is based on probabilities determined by the dimensions of the traps and their separations.

3.2. Simulation principle

The simulation accounts for the 3399-trap array of the microreactor. Particle position outside traps is defined in two dimensions only, (a) laterally, i.e., position transverse to the flow direction, and (b) axially, i.e., along the flow direction. An entering particle of catalyst appears in the inlet area before the first row of traps. The lateral position at entry is guided by a defined incoming particle flow distribution which specifies the probability of finding a particle as a function of position. Once a particle appears, it moves in the flow direction according to the probabilities below.

The probabilities of the motion of the particle moving through the field of traps (Fig. 6(b)) are defined as follows. The probability of the particle entering a trap is simply the ratio of the relevant geometric spacing:

$$P_{\text{trap}} = \frac{X_1}{X_2} \tag{6}$$

where the X_i is defined in Fig. 6(b). The probability of avoiding a trap by movement to the right or left is

$$P_{\text{left}} = P_{\text{right}} = \frac{1 - P_{\text{trap}}}{2} \tag{7}$$

Probabilities along the extreme edges of the bed are slightly different (Fig. 6(b)):

$$P_{\text{trap}} = \frac{X_1}{X_3 + X_4}, \qquad P_{\text{right}} = \frac{X_3}{X_3 + X_4}, \qquad P_{\text{left}} = \frac{X_4}{X_3 + X_4} \tag{8}$$

which apply to both sides of the bed.

The capacity of each trap is determined by modeling a 4-post trap with posts tapering from top to bottom as in Fig. 7. The post diameter is 35 μm as measured on top and 15 μm at the attachment to the wafer surface. Since the height of the tapered posts is ~300 μm and the average height of the particles is $\bar{c} = 27.1$ μm as described, the theoretical trap is made up of 11 layers.

For each layer within the stack, the number of particles that may be accommodated on a layer decreases somewhat with elevation. A geometrical model of the 11 layers of a single trap was

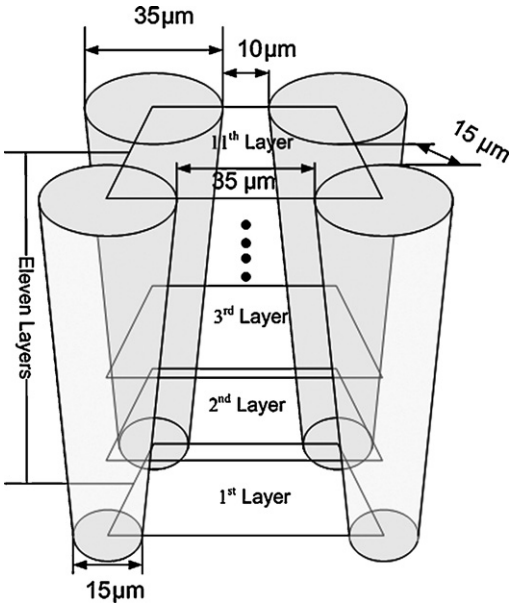

Fig. 7. The dimensions of the four-post trap which because of its height can contain multiple particles by layering. Based on the trap geometry and particle size, an 11-layer assumption was made in developing the particle filling model.

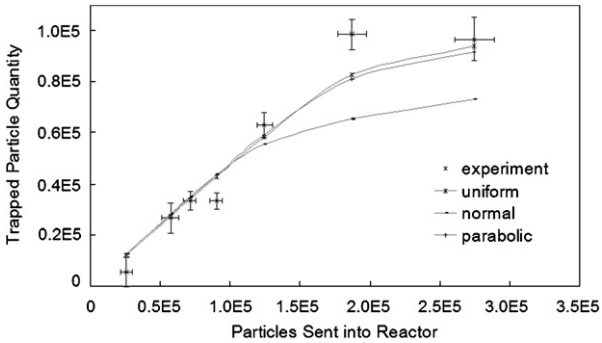

Fig. 8. Comparison of results of the simulation vs. loading experiments. Error bars are based on ±2 times the standard error. Curves resulting from the three different incoming particle flow distributions, uniform, normal and parabolic, are shown individually. The figure indicates that the uniform- and parabolic-flow distributions are most consistent with the experiment results.

developed, yielding a total of 29 particles as its maximum capacity which matched the experimental determination of capacity.

In the model, the probability of each particle becoming captured is affected by the variation of the aperture of entry to the trap for the 11 ascending layers resulting from the tapered structure of the posts. For example, as the first particle enters the first layer its probability (P_{trap}) of capture is calculated with Eqs. (6)–(8). The probability for the 2nd and 3rd particle entering the same 1st layer is $2/3P_{trap}$ and $1/3P_{trap}$ respectively since less room is available on a given layer as the layer becomes filled and the capacity of the layer was found to be 3 by geometrical considerations. The same rule governs the remaining 10 layers of each trap when the previous layer is filled. This approach is simplistic in its design as it treats particle entry and occupation as two dimensional despite the layering that occurs. However, there are no adjustable parameters in the model, it is based simply on the geometry of the reactor and particles, and simple probability Fig. 8 shows the experimental and simulated curves of the filling trials. Despite the simplicity of the model, the error bar calculated by combining uncertainties [24] indicates that, the experimental data presents a good correlation with the simulation, helping to support the basic probability mechanism.

4. Discussion and conclusion

4.1. Comparison of experiment and simulation

The two curves comparing the experimental results to the simulation (Fig. 8) are remarkably consistent, with both showing similar shape. Error bar length is calculated as twice the value of the standard error, reflecting a 95% level of certainty that the plotted points fall within the range shown on the graph. At low loading levels, the availability of trapping sites is high, so trapping efficiency is approximately constant, and the curve is linear. At higher levels of filling, trapping becomes progressively less efficient as the quantity of available sites diminishes. Consequently, the curve saturates as reactor capacity is approached.

The tapered posts result in a tapering of the aperture of entry to the trap. Based on measurements of SEM images, we determine that the entrance at the level of the wafer surface is 55 μm in width while the post spacing opposite the entrance (labeled "Exit" in Fig. 1(b)) is 20 μm. These openings are somewhat larger than the nominal design dimensions of 35 μm and 10 μm, respectively. Hence, for a particle size distribution in the range of 6–54 μm, entry is facilitated but so is the possibility of unplanned exit from the trap. At higher elevations in the trap, the probability of particle escape decreases, however, the ability for particles to escape at the lower levels will always be available. This geometry likely has a role in reducing filling efficiency somewhat as well as causing the tendency for a filled reactor to lose catalyst at some rate after filling.

This tapered post dimension diameter can also help explain the particle loss that we observed in the loading of individual traps monitored microscopically after each filling cycle. Detailed statistics on the occupancy on each of the 50 observed traps with each filling cycle reveal that although in general, traps accumulated particles with each successive filling, a few traps at random showed a decrease in trapped particles after a given cycle. There are various explanations possible for this behavior, including: (1) loss of particles through the tapered aperture as mentioned and (2) the creation of turbulence by excessive suctioning of particles, with the result that trapped particles could be ejected from a trap. In order to reduce the particle loss by either effect, we investigated the effects of reducing the vacuum suction. However, this resulted in the accumulation of a greater proportion of free particles in the reactor with the result that trapping ratio falls. Higher levels of suction normally sweep out the free particles, hence an optimum exists that balances particle loss and free particle accumulation.

4.2. Trap occupancy ratio as a measure of filling effectiveness

We have used the parameter of trap occupancy ratio, i.e., the fraction of traps having at least one particle, to assess filling effectiveness because of the ease in making quick estimates based on visual scanning of the reactor, with or without a microscope. Hence it is a rapid but crude means of assessment. As indicated in the introductory section, the particle loading investigation was initiated because we observed the trap occupancy to be ≈20% during the hydrogenation reaction experiments described in Section 1.2. Based on microscope imaging in the filling experiments, 49 of 50 traps were occupied, meaning the trap occupancy ratio achieved was 98%, a significant increase. This improvement is clearly correlated to a greater attention to matching trap dimensions to particle size distributions using the sieving procedure above.

4.3. Particle capture distributions based on visual sampling and investigating incoming flow distributions

In the simulation it was necessary to designate the initial location of a particle upon entrance to the reactor. We ran simulations with three different particle located distributions which are based on possible fluidized flow dynamics of the incoming particles. The three incoming particle flow distributions: (1) the uniform distribution, i.e., the probability of finding a particle along the traverse axis is constant; (2) the normal distribution, wherein the probability of finding a particle is greater in the center of the flow channel and drops off toward the edges, similar in shape to a Gaussian or normal distribution "bell curve"; (3) the parabolic distribution, similar to the normal distribution but without inflection points from the center of the flow channel to the wall. The motivations behind each of the distribution were as follows; note that the distribution was applied only in the open entry area which is free of obstacles:

(1) The uniform distribution is the simplest meaningful function that could be specified. It is similar to "plug flow" and is generally used to simulate the time-averaged velocity profile in turbulent flow [25]. However, the catalyst-trap reactor is expected to operate in laminar flow based on low Reynolds Number [25].
(2) The normal distribution was arbitrarily chosen for simulation as it provides a mathematical description that places a greater probability of finding a particle towards the center of the flow passage. The inflection points toward the outer extremes of the flow path are not present in known velocity profiles and hence it was suspected at the outset that inaccuracy could arise from this behavior.
(3) The parabolic distribution is the one most correlated to the physical system. A parabolic velocity distribution is expected for the laminar flow [25] situation that was expected to develop. Moreover, since transitions from the flow supply line to the reactor are gently tapered, it is expected that flow would be fully developed at the entry, with the result that we would expect the parabolic profile to govern.

The results of the three simulations compared to the experimental data are shown in Fig. 8. Here we see relatively close agreement between experiment and simulation for the uniform- and parabolic-function based simulations. The reasonably close agreement between experiment and simulation is a validation of the basic probabilistic mechanism adopted in the model.

When the reactor is less than about 50% filled (i.e., 0.5E5 on the vertical axis of Fig. 8), all three distributions follow the same curve

in Fig. 8. Under these conditions, empty sites for catalyst particles are plentiful and incoming particles can easily find a position to lodge themselves.

At filling above about 50%, interestingly, the two simulation results for uniform and parabolic do not significantly differ from one another, whereas the normal distribution-based simulation indicates an inability to achieve reactor filling for the given particle input, i.e., a much lower trapping efficiency. This behavior is an artifact of the too drastic reduction in the entering probability density at intermediate distance from the reactor centerline. If the particle flow is too concentrated near the centerline, traps along this axis will tend to fill and trapping rates will drop off as there is insufficient particle flow at the outer extremes to fill up the traps there at a reasonable rate.

The fact that the uniform and parabolic distribution results do not differ significantly from one another at high filling (>50% filled) is due to the actual shape of the parabola implemented. By suitable selection of the parameters defining the parabola, a sharper or less sharp profile will be formed. The parabola that produced the curve in Fig. 8 was relatively broad, and approaches the uniform distribution in result. A more peaked parabolic distribution would approach the normal distribution result more closely.

The ability of particles to escape from traps due to the broadened aperture from tapered posts was not specifically accounted for in the modeling mechanism. Nevertheless, this did not negatively influence agreement with experiment. From this we conclude that the stochastic mechanism accounts for a certain fraction of untrapped particles passing through the reactor since the probability of capture is not 100%. The agreement seen in Fig. 8 suggests that the escape of particles from traps, which is known to occur, must not be the dominant effect in trapping efficiency.

4.4. Conclusion

The particle filling of the catalyst-trap microreactor was shown to be understandable by a simple mechanism where probability of capture in a trap is determined by the relevant geometry in the reactor catalyst bed. Further validation of this mechanism could be achieved by constructing reactors of varying geometry and assessing their trapping efficiency. The achievement of 98% trap occupancy ratio suggests that this filling approach has viability for implementation with the catalyst-trap microreactor for real organic synthetic applications.

Although loading gave less than 100% filling efficiency, the waste of the catalyst was negligible due to the μg-scale of the experiments. In an industrial setting, we anticipate that a procedure involving recycle of the outlet suction stream would be possible for reducing waste. While not the dominant factor in trapping inefficiency, the tapered posts of the reactor which come about through process settings in the DRIE technology used in microfabrication, could be eliminated by optimization. Moreover, a narrowing of the particle size distribution through smaller mesh, high quality sieves, could also improve trapping. Implementation of these measures could lead to further improvement in trapping efficiency.

Nomenclature

$\bar{L}$	Mean length of the catalyst particle
$\bar{W}$	Mean width of the catalyst particle
V_p	Average catalyst volume based on ellipsoid volume calculation
ρ	Density of 5 wt.% Pd/C catalysts after sieving
r_{trap}	The proportion of the quantity of particles trapped to the quantity of particles stay in the reactor
η_{trap}	The proportion of the mass of particles trapped to the mass of particles send in the reactor
N_{in}	The quantity of particles sent into the reactor
N_{trap}	The quantity of particles trapped in the reactor
W_{in}	The weight of total catalysts sent into the microreactor
W_{reac}	The weight of catalyst staying in the reactor after vacuuming twice
$W_{reactor}$	The weight of microreactor
n_{trap}	The quantity of particles trapped based on 50-trap sampling
n_{free}	The quantity of particles trapped based on 50-trap sampling
P_{trap}	Probability of particles been trapped
$P_{left/right}$	Probability of particles bouncing to left/right of a trap

Acknowledgements

The authors gratefully acknowledge the skillful assistant of simulation by Sheng Chen and Yuyang Zhang in the Department of Electrical Computer Engineering of Stevens Institute of Technology and the helpful suggestions of Elizabeth Lennon, Peter Lindner, Ayokunle Omosebi and Sang Youp Hwang in the Department of Chemical Engineering and Materials Science of Stevens Institute of Technology.

References

[1] S. McGovern, G. Harish, C.S. Pai, W. Mansfield, J.A. Taylor, S. Pau, R.S. Besser, Multiphase flow regimes for hydrogenation in a catalyst-trap microreactor, Chem. Eng. J. 135 (2008) S229–S236.
[2] P. Watts, C. Wiles, Recent advances in synthetic micro reaction technology, Chem. Commun. (2007) 443–467.
[3] R.S. Besser, X. Ouyang, H. Surangalikar, Hydrocarbon hydrogenation and dehydrogenation reactions in microfabricated catalytic reactors, Chem. Eng. Sci. 58 (2003) 19–26.
[4] B.K. Singh, C.V. Stevens, D.R.J. Acke, V.S. Parmar, E.V. Van der Eycken, Copper-mediated N- and O-arylations with arylboronic acids in a continuous flow microreactor: a new avenue for efficient scalability, Tetrahedron Lett. 50 (2009) 15–18.
[5] K. Koch, R.J.F. van den Berg, P.J. Nieuwland, R. Wijtmans, M.G. Wubbolts, H.E. Schoemaker, F.P.J.T. Rutjes, J.C.M. van Hest, Enzymatic synthesis of optically pure cyanohydrins in microchannels using a crude dell lysate, Chem. Eng. J. 135 (2008) 89–92.
[6] J. Choe, J.H. Seo, Y. Kwon, K.H. Song, Lithium–halogen exchange reaction using microreaction technology, Chem. Eng. J. 135 (2008) S17–S20.
[7] M. Margulies, M. Egholm, W.E. Altman, S. Attiya, J.S. Bader, L.A. Bemben, J. Berka, M.S. Braverman, Y. Chen, Z. Chen, S.B. Dewell, L. Du, J.M. Fierro, X.V. Gomes, B.C. Godwin, W. He, S. Helgesen, C.H. Ho, G.P. Irzyk, S.C. Jando, M.L.I. Alenquer, T.P. Jarvie, K.B. Jirage, J. Kim, J.R. Knight, J.R. Lanza, J.H. Leamon, S.M. Lefkowitz, M. Lei, J. Li, K.L. Lohman, H. Lu, V.B. Makhijani, K.E. McDade, M.P. McKenna, E.W. Myers, E. Nickerson, J.R. Nobile, R. Plant, B.P. Puc, M.T. Ronan, G.T. Roth, G.J. Sarkis, J.F. Simons, J.W. Simpson, M. Srinivassan, K.R. Tartaro, A. Tomasz, K.A. Vogt, G.A. Volkmer, S.H. Wang, Y. Wang, M.P. Weiner, P. Yu, R.F. Begley, J.M. Rothberg, Genome sequencing in microfabricated high-density picolitre reactors, Nature 437 (2005) 376–380.
[8] H. Surangalikar, X. Ouyang, R.S. Besser, Experimental study of hydrocarbon hydrogenation and dehydrogenation reactions in silicon microfabricated reactors of two different geometries, Chem. Eng. J. 93 (2003) 217–224.
[9] K. Schubert, J. Brandner, M. Fichtner, G. Linder, U. Schygulla, A. Wenka, Microstructure devices for applications in thermal and chemical process engineering, Microsc. Thermophys. Eng. 5 (2001) 17–39.
[10] A.J. deMello, Control and detection of chemical reactions in microfluidic systems, Nature 442 (2006) 394–402.
[11] T. Schwalbe, V. Autze, G. Wille, Chemical synthesis in microreactors, Chimica 56 (2002) 636–646.
[12] H. Lowe, W. Ehrfeld, State-of-the-art in microreaction technology: concepts, manufacturing and applications, Electrochim. Acta 44 (1999) 3679– 3689.
[13] S. Lobbecke, W. Ferstl, S. Panic, T. Turcke, Concepts for modularization and automation of microreaction technology, Chem. Eng. Technol. 28 (2005) 484–493.
[14] W. Ferstl, S. Loebbecke, J. Antes, H. Krause, M. Haeberl, D. Schmalz, H. Muntermann, M. Grund, A. Steckenborn, A. Lohf, J. Hassel, T. Bayer, M. Kinzl, I. Leipprand, Development of an automated microreaction system with integrated sensorics for process screening and production, Chem. Eng. J. 101 (2004) 431–438.
[15] V Hessel, C Knobloch, H Lowe, Review on patents in microreactor and micro process engineering, Recent Patents Chem. Eng. 1 (2008) 1–16.

[16] R. Chapanian, M.Y. Tse, S.C. Pang, B.G. Amsden, The role of oxidation and enzymatic hydrolysis on the in vivo degradation of trimethylene carbonate based photocrosslinkable elastomers, Biomaterials 30 (2009) 295–306.
[17] S. Odisitse, G.E. Jackson, In vitro and in vivo studies of the dermally absorbed Cu(II) complexes of N_3O_2 donor ligands—potential anti-inflammatory drugs, Inorg. Chim. Acta 362 (2009) 125–135.
[18] T.M. Squires, S.R. Quake, Microfluidics: fluid physics at the nanoliter scale, Rev. Mod. Phys. 77 (2005) 977–1076.
[19] G.N. Doku, W. Verboom, D.N. Reinhoudt, A. van den Berg, On-microchip multiphase chemistry—a review of microreactor design principles and reagent contacting modes, Tetrahedron 61 (2005) 2733–2742.
[20] H. Tietze, Famous Problems of Mathematics: Solved and Unsolved Mathematics Problems from Antiquity to Modern Times, New York, Graylock Press, 1965, pp. 40–41.
[21] M.J. Madou, Fundamentals of Microfabrication: The Science of Miniaturization, second ed., Taylor & Francis, New York, 2002, pp. 535–614.
[22] A.D. Chepelianskii, D.L. Shepelyansky, Dynamical turbulent flow on the Galton Board with friction, Phys. Rev. Lett. 87 (2001) 034101–34111.
[23] V.V. Kozlov, M.Y. Mitrofanova, Galton board reg, Chaotic Dynam. 8 (2002) 431–439.
[24] D.C. Baird, Experimentation: An Introduction to Measurement Theory and Experiment Design, second ed., Prentice-Hall, New Jersey, 1988.
[25] N. de Nevers, Chem. Engineering Series: Fluid Mechanics for Chemical Engineers, McGraw-Hill, Boston, 1991.